Characteristic losses in metals: Al, Be, and Ni

H. H. Madden, R. Landers, G. G. Kleiman, and D. M. Zehner

Articles you may be interested in

Soft x-ray appearance potential spectroscopy study of MgO (100) and -Al2O3 (100) single crystals
J. Vac. Sci. Technol. A **31**, 06F110 (2013); 10.1116/1.4828785

Structure of hydrogen-dosed graphene deduced from low electron energy loss characteristics and density functional calculations
Appl. Phys. Lett. **97**, 253118 (2010); 10.1063/1.3526373

Oxygen-induced changes in electron-energy-loss spectra for Al, Be and Ni
J. Vac. Sci. Technol. A **17**, 2719 (1999); 10.1116/1.581936

Auger electron spectroscopy and electron energy loss spectroscopy study of the adsorption of nitrogen on a polycrystalline zirconium surface
J. Vac. Sci. Technol. A **15**, 2548 (1997); 10.1116/1.580768

Introduction to the Surface Spectra of Oxides
Surf. Sci. Spectra **4**, 181 (1996); 10.1116/1.1247792

Characteristic losses in metals: Al, Be, and Ni

H. H. Madden, R. Landers,[a] and G. G. Kleiman
Instituto de Física ''Gleb Wataghin'', Universidade Estadual de Campinas (UNICAMP),
Caixa Postal 6165, 13081-970 Campinas, São Paulo, Brasil

D. M. Zehner[b]
Solid State Division, Oak Ridge National Laboratory, Oak Ridge, Tennessee 37831-6057

Information about the *occupied* portion of the surface density of states of materials can be derived from electron-excited Auger electron spectroscopy (AES), which is a standard experimental technique in most surface science laboratories. Surface sensitive experimental techniques that provide information regarding the *unoccupied* portion of the surface density of states are often not standard and are not so readily available. Here we explore the possibility of utilizing the same experimental equipment as in AES to derive information about the unoccupied portion of the surface density of states from a characteristic loss spectroscopy, in particular, from core-level inelastic electron-scattering spectroscopy (CLIESS). An important application of this technique is in comparative studies. CLIESS spectra from clean surfaces of aluminum, beryllium and nickel are presented. These data were taken in the first-derivative mode using the reflection of monoenergetic primary beams of 450 eV energy for Be, and 300 eV for Al and Ni. The Al and Be spectra had to be extracted from overlapping plasmon signals using synthesized plasmon spectra based on the behavior of these spectra between the elastic peak energy and the respective core level threshold energies. After applying loss-deconvolution techniques to remove secondary loss spectral distortions, integral spectra were obtained which compared well to corresponding experimental soft x-ray absorption and transmission electron-energy loss data as well as to theoretical calculations of the unoccupied density-of-states for these materials. Comparison similarities as well as some differences are discussed. Finally, in order to illustrate the potential these signals have in serving as ''fingerprints'' of surface chemistry, derivative metal-CLIESS curves for the three oxide surfaces of the metals are also presented. © *1998 American Vacuum Society.* [S0734-2101(98)00504-1]

I. INTRODUCTION

When a beam of slow, monoenergetic electrons is directed at the surface of a solid, some will undergo energy losses involving electronic transitions. For very low primary beam energy, these losses involve either collective excitations of the valence electrons or low-energy interband transitions. These excitations in electron-energy-loss spectroscopy (EELS) are termed plasmon losses[1] and interband-transition losses,[2] respectively. They can be investigated using equipment common in any laboratory setup to study solid-state surface phenomena, or to perform routine surface analyses.

For a given material, new energy-loss channels are opened as the energy of the primary beam increases. These can have sharp thresholds as the primary electron energy becomes just sufficient to excite core-level electrons to empty conduction band (CB) levels, which are just above the Fermi energy in metals. (In the following, it is to be understood that the empty CB density of states we mention is that in the presence of a core hole. This might modify its nature considerably from that in the ground state of the metal.) Since these losses involve definite core electrons in fairly narrow levels and because of the abrupt transition between occupied and empty levels (at the Fermi energy in metals),

sharp threshold signals are seen in EELS. EELS measurements involving these characteristic losses may be termed core-level inelastic electron scattering spectroscopy (CLIESS). With increasing primary beam energy, transitions occur to higher lying CB levels. Thus, in principle, the shapes of the CLIESS signals contain CB unoccupied density-of-states (DOS) information. In early experiments, such information was sought mostly in soft x-ray absorption spectroscopy (SXAS) measurements[3] and work along these lines has increased with the increasing availability of synchrotron light sources.[4] CB DOS information is, however, also readily available in EELS measurements.[5–8]

Studies of plasmon losses have been concentrated most often on those light metals, e.g., Al, Mg, Na and Be, for which such losses are theoretically expected[1]. For these metals, the plasmon loss spectrum from aluminum is perhaps the most widely investigated.[9–13] This is because of the clear (nearly) free-electron metal character of Al, of its strong plasmon-loss signals, and of its importance in industry. There is also of course the fundamental interest in these losses themselves and in what portion of the plasmon features seen both in x-ray photoemission spectroscopy (XPS) and auger electron spectroscopy (AES) can be attributed to intrinsic (coherent) plasmon creation as opposed to extrinsic (incoherent) plasmon creation.[9,10] Both of these mechanisms have practical importance in making XPS more useful for quantitative surface analyses of solids. We will see, further

---

[a]Author to whom correspondence should be addressed; electronic mail: landers@ifi.unicamp.br

on, that the strong plasmon loss signals present complications in the study of CB DOS information from CLIESS-signal line shapes.

This article is concerned with the results of EELS measurements involving medium energy electrons, 100 eV ≤ primary energy ≤ 500 eV, and using only the energy resolution provided by conventional surface analysis equipment more generally used for AES. The EELS information can obviously be obtained using higher primary energies in a transmission mode if the sample is thin enough, but for studies of metals, semiconductors and some insulating materials, the reflection mode with medium energy electrons provides a convenient complement to other surface analysis techniques and is, by its very nature, surface sensitive. The three metals studied are representative of ''free-electron-like'' (Al and Be, because of their strong plasmon signals) and d-band metals (Ni). Changes in surface CB DOS can be readily recognized using CLIESS measurements without applying the data processing techniques we describe here. This technique is therefore suitable for comparative studies.

The fact that the energy location of CLIESS signals can be shifted by simply changing the energy of the exciting electrons makes this technique of practical use in cases where overlapping AES signals may result in unresolved questions in surface analyses. In XPS the photoemission signals are similarly tied to the energy of the exciting particles. Thus, in principle, these signals could also be moved to any position in the energy spectrum. In most laboratory systems, however, a limited number of x-ray sources, one or two with nontunable energies, are available. Therefore, the XPS signals from these systems are as restricted in energy location (or almost so in the case of two sources) as the AES signals.

The primary concern in this article will be with the extraction of CB DOS information from CLIESS and how it compares with the results of other experimental probes of the CB DOS for these materials, as well as with theoretical DOS calculations. The reliability of the CB DOS information contained in our processed CLIESS data is demonstrated in these comparisons. For Al and Be the plasmon-loss spectrum had to be synthesized in order to separate it from the CLIESS signal. This synthesis will be discussed in terms of the efforts of others to do similar syntheses for Al and Be.[9–11]

II. EXPERIMENT

All three types of samples were polycrystalline. The Al and Ni samples were thin films evaporated *in situ* onto a thin tungsten foil substrate. By flashing the W foil to temperatures ≥ 2500 K, it was possible to produce a clean substrate without detectable AES signals from surface contaminants. Thus, when measurements on an Al or Ni film were completed, fresh films could be deposited onto the clean W substrate. For clean film deposition, evaporation was continued until the substrate signal had disappeared, and the sample was cut from 5 N purity bulk stock. Its surface was cleaned by conventional argon ion bombardment and annealing techniques. The cleanliness of the surfaces was monitored using AES. XPS measurements were also made on the Be sample
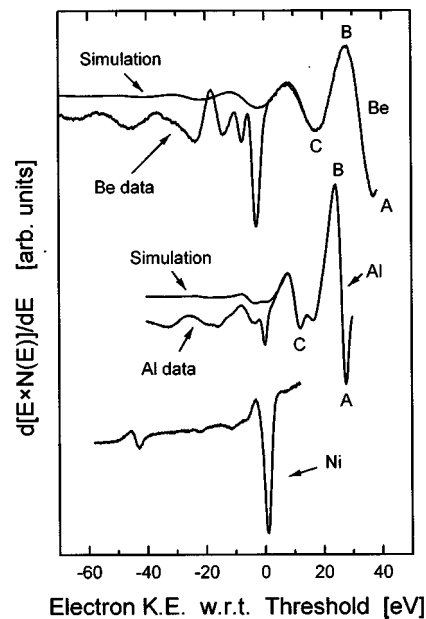

FIG. 1. Electron-energy-loss spectra in the first-derivative mode for Be, Al and Ni. The abscissa gives energy-loss values referenced to the Be(K), Al(L_{23}) and Ni(M_{23}) core-level (binding energy) thresholds, respectively.

to provide reference values for the AES and CLIESS measurements. Oxygen was the only AES-detectable surface contaminant that built up during measurements. The working pressure in our vacuum systems during data acquisition was less than 3×10^{-8} Pa.

Cylindrical-mirror analyzers (CMAs) were used to measure the EELS data—a single-pass CMA for the Al and Ni measurements, and a double-pass CMA for the Be measurements. These measurements were all taken in the derivative mode, $d(E \times N(E))/dE$, that is commonly used with these analyzers for AES measurements. Thus the integral data first had to be corrected for the energy dependence of the analyzer transmission. The modulation voltage was 1 V_{pp}. Signal averaging was used to obtain spectra with a signal-to-noise ratio greater than 25 in most cases.

III. DATA PROCESSING

Raw derivative spectral data are shown in Fig. 1. Nominally, the primary energy, E_p, is 300 eV for excitation of the Al(L_{23}) and Ni(M_{23}) signals; and 450 eV for the Be(K) signal. Characteristic features are evident in these pre-processed, derivative data. The primary purpose of our data processing is that of controlling only the shapes of the gross features in the integrated signals. The relative energy values in this and in later plots were calculated in each case by first subtracting the primary beam energy from the analyzer energy values and then adding a value equal to the XPS binding energy for the core line involved. The binding energy values [72.6 eV for Al(L_{23}); 111.5 eV for Be(K); and 67 eV for Ni(M_{23})] were taken from published literature, although for Be the value was checked using the XPS capabilities of the double-pass CMA system. (Since our primary interest
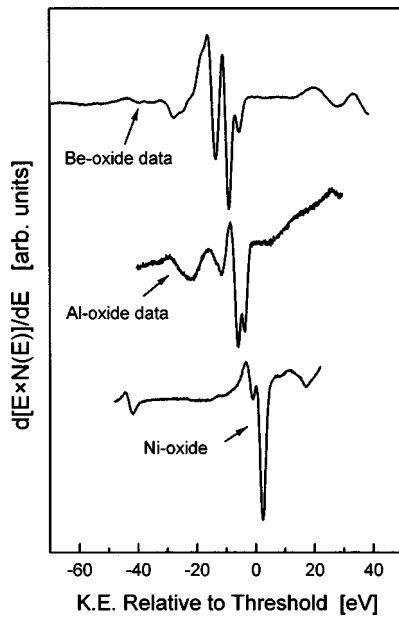
FIG. 2. Electron-energy-loss spectra, in the (uncorrected) first-derivative mode, for oxidized surfaces of Be, Al and Ni. The abscissa gives relative energies referenced to the *clean surface* core-level binding energies for Be(K), Al(L$_{23}$) and Ni(M$_{23}$).

was in signal line shapes, no special care was given to the accuracy of either the analyzer energy scale or the meter reading of the primary-beam energy setting. For AES, the primary function of the single-pass system, the latter is not important.)

While the actual measured electron kinetic energies for the characteristic features in the spectra in Fig. 1 may be used to distinguish elemental signals, the *shapes* of the spectra are also different from one another. This makes a clear identification of a given clean metal surface even more distinctive. Figure 2 gives plots of the same three metal-CLIESS curves for oxide surfaces. Comparing the shapes of the clean and oxide signals for a given metal one sees that the CLIESS shapes very clearly reflect changes in the chemical state of the surface. A more detailed report of the effects of oxygen on the shapes of EELS signals from these three metals, both CLIESS and plasmon-loss signals, will be the subject of an article that is currently in preparation.[14] Although core-level threshold energies are most certainly changed by oxidation, the clean surface values were used for calculating the "relative energies" in Fig. 2. This allows an assessment of the "chemical shifts" brought about by oxidation. These data demonstrate that CLIESS signals can provide an alternative source of clear-cut surface chemistry information, complementing AES or XPS signals in this role.

In pure Al and Be, the incident electron loses energy through emission of discrete numbers of bulk and surface plasmons, represented by a plasmon loss signal, I_p. For losses greater than the binding energy of the relevant level, ionization is possible and the CLIESS characteristic loss signal, I_c, appears. When a sufficiently high number of plasmons is emitted, the CLIESS signals of Al and Be are super-

imposed on the plasmon-loss spectra: the impossibility of separately measuring the plasmon and CLIESS signals in the threshold region is clear.

In order to extract the CLIESS signals, it is necessary to provide a synthesized, derivative plasmon-loss spectrum in the CLIESS-energy range. Because of its importance in attempts at identifying intrinsic plasmon production associated with photoelectron emission[9,10] and in efforts at making XPS a more reliable quantitative analysis technique,[11] the problem of synthesizing the plasmon spectrum has been addressed a number of times previously in XPS studies.

It is important to realize that accurate representations of the separate bulk- and surface-component line shapes appropriate to our experimental situation are needed in order to construct a truly accurate synthesized plasmon spectrum. Previous syntheses of the overall $I_p(E)$ spectrum have been performed in other applications.[9–11] Of these, that which most closely meets our requirements is related to analysis of XPS data. There are, however, some important differences between the XPS experiments[11] and those reported here: (1) The synthesized $I_p(E)$ curves in XPS produce agreement with the measured data which, although quite adequate when comparing integral intensities,[11] exhibit small departures from the experimental data which are magnified in the derivative spectra, giving rise to erroneous structure rivaling or overwhelming the CLIESS signal in strength. (2) The XPS experiments produce photoelectrons whose kinetic energies are so high that they are relatively insensitive to the surface, so that the surface plasmon contribution to the loss spectra is relatively unimportant[11]—our incident electrons have kinetic energies close to those corresponding to the minimum in the mean free path, so that they are sensitive to the surface and the surface plasmon component of the loss spectra is important. This is clearly seen in the Be and Al curves in Fig. 3, where we present the integral spectra (above the CLIESS region) corresponding to the derivative spectra in Fig. 1: the magnitude of the first surface plasmon is clearly illustrated. (3) Finally, the very nature of the XPS and CLIESS experiments are different. In XPS, coupling of the valence band electron gas to the core hole produces, in the loss spectra, intrinsic plasmon contributions and asymmetry effects induced by electron-hole pair creation.[11] These core hole associated effects are, in addition to extrinsic plasmon production, the only contribution in CLIESS which involves no core holes for loss energies above threshold. Neglecting multiple surface plasmon production, the form of the background subtracted extrinsic plasmon loss spectrum (to which a background should be added) is given in Eq. (1)[11]

$$I_p(E) = \sum_{n=0} G_n(E), \tag{1a}$$

$$G_n(E) = aD_B(E) \otimes G_{n-1}(E), \tag{1b}$$

$$G_0(E) = (1 - a_{sp})I_0(E) + a_{sp}d_{sp}(E) \otimes I_0(E), \tag{1c}$$

where a and a_{sp} are the probabilities of emission of bulk and surface plasmons, respectively, and I_0 is the incident intensity. The bulk and surface plasmon resonance line shapes are
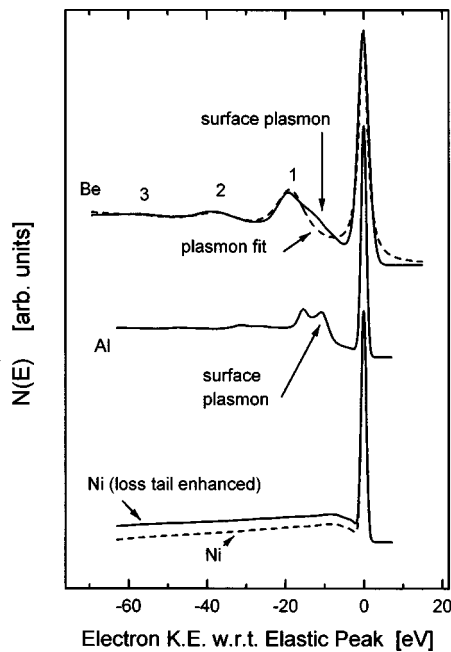
FIG. 3. Integral, $1/E$ corrected backscattered EELS curves used in loss deconvolution for Be, Al and Ni. The elastically backscattered electron peaks are centered on the abscissa zero. The dashed curve for Ni gives the data before the scaling that was done on the loss tail. Those points on the right hand side of each curve are at zero. The plasmon peaks are numbered in accordance with their citations in the text.

denoted by D_B and d_{sp}, respectively. The symbol $\otimes$ denotes convolution. The profile in Eq. (1a) corresponds, therefore, to the sum of extrinsic plasmon peaks, each of which is a convolution of its predecessor with the bulk plasmon resonance line shape. Each such peak consists of a portion derived from the incident intensity and one originating in the surface plasmon resonance. The form of Eqs. (1) illustrates the difference from XPS analysis:[11] the absence of a core hole in the initial state of CLIESS obviates the necessity of including intrinsic plasmon production and electron-hole pair produced asymmetries.

Approximating the peaks by Lorentzian line shapes, and defining the energies relative to the primary energy, we have

$$G_0(E) = c_0 L(E, \gamma) + c_0^{sp} L(E + \hbar\omega_{sp}, \gamma + \Gamma_{sp}), \qquad (2a)$$

$$G_n(E) = c_n L(E + n\hbar\omega_B, \gamma + n\Gamma_B)$$
$$+ c_n^{sp} L(E + \hbar\omega_{sp} + n\hbar\omega),$$

$$L(x, \Gamma) \equiv \frac{\Gamma/\pi}{(x^2 + \Gamma^2)},$$

$$c_n \equiv a^n(1 - a_{sp}); \quad c_n^{sp} \equiv a^n a_{sp}. \qquad (2b)$$

In Eqs. (2), we have represented the incident intensity width by γ, and that of the bulk and surface plasmons by Γ_B and Γ_{sp}, respectively. The bulk plasmon losses occur, therefore, at loss energies $n\hbar\omega_B$ below the primary energy, with associated surface plasmon replicas at loss energies $n\hbar\omega_B + \hbar\omega_{sp}$. The respective widths are $n\Gamma_B + \gamma$ and $n\Gamma_B + \gamma + \Gamma_{sp}$.

From the form in Eqs. (1) and (2), it appears possible to fit the plasmon profile for energies greater than the CLIESS region, a fit which could be extended into the CLIESS region. After all, the bulk and surface plasmon energies and widths have been characterized for Be and Al in energy loss experiments.[15] Such a fit was applied to Be and Al XPS data[11] to determine the bulk and surface plasmon energies, widths and the coefficients c_n and c_n^{sp} of the plasmon resonances in Eqs. (1) and (2), with results in agreement with energy loss studies.[15] Application of this procedure to spectra such as those in Fig. 3, however, is not unambiguous: the spectra can be fit with a wide range of the parameters. The situation is illustrated in Fig. 3 where the measured Be spectrum outside the first surface plasmon region is shown to be virtually indistinguishable from a simulation considering only bulk plasmons (i.e., $a_{sp}=0$) of energy ($\hbar\omega_B=18.5$ eV) and width ($\Gamma_p=7.0$ eV) determined from energy loss experiments[15] and adjustable coefficients, $c_1=1.99$, $c_2=0.76$ and $c_3=0.32$, whose relation deviates from that given in plasmon profiles of the form of Eqs. (2). The reason for this difficulty is attributable to the strong Be surface plasmon, whose effect is simulated by changing the weights of the bulk plasmons to values which are probably incorrect. Inclusion of multiple surface plasmon emission would appear to be indicated. A similar difficulty was observed in fitting XPS data for Na $1s$, whose photoelectrons have kinetic energy $\cong 300$ eV and are also surface sensitive.[11] A more complete characterization of the surface plasmons, which is outside the scope of this article, is probably indicated in order to better describe the data.

Given this situation, we adopt the frankly empirical approach of applying the regularity of the plasmon profile expression in Eqs. (1) and (2) to the total derivative mode data in Fig. 1: the n plasmon peak bears the same relation to the $n+1$ as the $n+1$ does to the $n+2$. Determination of this relation allows us to extend the plasmon simulation into the CLIESS region. The empirical prescription for treatment of the plasmons determined in this way may be applicable more widely.

Since the Be CLIESS threshold occurs at a greater loss energy than that of Al, the Be plasmon signals have had more of a chance to decay before the onset of the CLIESS signal than in the case of Al. From our previous discussion, for Be the surface component of the plasmon spectrum was found to be discernible only very close to the elastic peak as in Fig. 3. The rest of the plasmon spectrum between the elastic peak and the threshold of the Be(K)-CLIESS signal behaves as though it consisted of only one component—the bulk plasmon—and the successive multifold convolutions[9–11] of that single component in our discussion we shall denote as "bulk plasmons." In the derivative mode in which our synthesis was done, the spectrum was more or less a sinusoidal curve with decaying amplitude. Finally, of the three raw spectra in Fig. 1, the characteristic loss structure of the Be signal is the strongest and most well defined. These features make the task of generating a reasonably good syn-
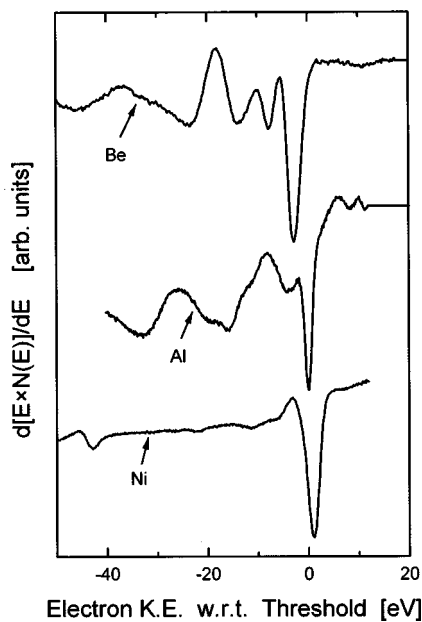
FIG. 4. CLIESS spectra for Be(K), Al(L_{23}) and Ni(M_{23}) in the derivative mode after removal of the overlapping plasmon-loss spectra for Be and Al. The conventions are those of Fig. 1. The data points on the high-energy side of threshold for each curve were set to zero average value before integration.

thesized continuation of the Be plasmon spectrum a relatively easy task.

Utilizing the notation for the plasmon structures embodied in Fig. 1: A-B-C, means minimum-maximum-minimum, we observe that third ''bulk plasmon'' of Be could be derived from the second, and the fourth from the third by the following procedure: (a) we split the 2nd ''bulk plasmon'' structure, for example, into two parts, minimum-maximum and maximum-minimum; (b) we scale these two parts separately with factors $(3.1)^{-1}$ and $(3.4)^{-1}$, respectively, and shift the scaled segments to greater loss energies by $\hbar\omega_B$; and (c) we adjust only the vertical positions of the segments for a smooth fit to the measured 3rd plasmon structure. This empirical procedure reproduces the 3rd and 4th experimental plasmon structures very well.

For Be, therefore, we formed the synthesized plasmon-loss spectrum in the CLIESS-energy ''window'' by taking the structure of the 4th Be plasmon loss (denoted by A-B-C minimum-maximum-minimum in Fig. 1) as a template, repeatedly scaling (as we describe above) and shifting its segments by integer multiples of $\hbar\omega_B$, the Be bulk plasmon energy, and aligning the shifted segments vertically until a smooth analytic continuation was obtained. This synthesized curve is shown in Fig. 1 along with the as-measured total spectrum. The derivative CLIESS spectrum in Fig. 4 was obtained by subtracting this synthesized spectrum from the total spectrum.

The analysis of Be is instructive, in that it makes clear that this procedure works well when (a) the CLIESS threshold occurs at a relatively large loss energy; and (b) the spectrum appears to be describable in terms of ''bulk plasmons.'' In the case of Al, these conditions are not properly met. The

Al(L_{23}) threshold occurs at a smaller loss energy than in Be and there are at least two signal components, presumably the bulk and surface plasmons, that persist throughout the plasmon spectrum. For this reason, the procedure described above, when applied in an unmodified form, does not work as well for the Al plasmon-loss spectrum.

For the reasons discussed above, it was not sensible to try to separate the surface and bulk plasmons in the loss structures of our Al films; detailed characterization of the surface plasmons would be indicated.[11] Consequently, we formed our Al plasma-loss synthesized spectrum in the CLIESS region by applying the Be procedure: the last complete (3rd) plasma structure (A-B-C in Fig. 1) occurring before the CLIESS threshold was used as a template which was replicated with empirical scaling factors determined by the relations between the respective halves of the 2nd and 3rd plasmon structures. The first maximum of this synthesized curve was too narrow to fit the final maximum before threshold in the total spectrum well. The features in the synthesized curve were therefore broadened by convolution with a 53 point ($\sim$6.37 eV full width) Savitzky–Golay smoothing array.[16] The simulation curves for both Al and Be are shown in Fig. 1.

The extracted Be(K) and Al(L_{23}) CLIESS spectra are plotted along with the Ni(M_{23}) CLIESS curve in Fig. 4. These curves were first numerically integrated. (While it goes without saying, it is important for subsequent processing that the data for a given spectrum be taken with constant energy separation between adjacent points.) Before integration a constant was added to, or subtracted from, the data points of a file so that the average value of 10 points or so just above the CLIESS threshold (in energy) was zero. The integration then proceeded from these points to lower energy. The points in this integrated signal were then divided by their corresponding energy value in order to correct for the $E \times N(E)$ transmission characteristics of the CMA analyzer. Loss-deconvolution techniques[17,18] were then applied to correct this $N(E)$ integral spectrum.

We should mention that the data represented in Fig. 4 correspond to I_c mentioned earlier. This quantity corresponds to a convolution between the spectrum of initial electrons which have lost an energy greater than the binding energy and that of electrons excited to the conduction band, *in the presence of core hole*. In our treatment, matrix element effects are neglected and we assume that the spectrum of inelastically scattered electrons is the same as that measured near the primary energy. The effects of the core hole and the neglect of matrix elements is not clear. In fact, a theoretical derivation including these effects does not exist in the literature.

The loss-deconvolution was performed using the van Cittert algorithm[18,19] that has demonstrated its success in correcting for similar distortions in AES line shapes.[20] Since, in contrast with AES, the CLIESS signal could not be expected to go to zero in the 40–50 eV region following threshold, we made no background correction to any of the signals other than the simple zero suppression of the high energy end be-
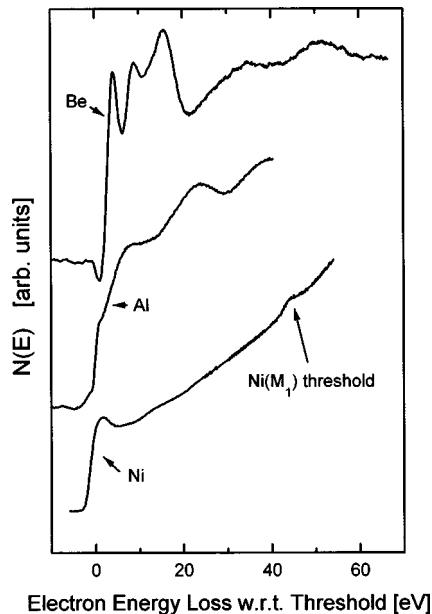
FIG. 5. Loss-deconvolution, integral CLIESS curves for Be(K), Al(L$_{23}$) and Ni(M$_{23}$). Note that for Ni the Ni(M$_1$) threshold is also visible. The energy losses are referenced to the Fermi energy. Before loss deconvolution, all curves were corrected for the CMA transmission characteristics after integration of the data in Fig. 4. The zero level for each curve is to be found on the left-hand side of each in this figure.

fore integration, as noted above. (There is no clear-cut criterion available for determining the correct background in the case of CLIESS.[19]) In addition, the CLIESS extraction procedure for Al and Be also contributes to the uncertainty in the background signal. The resulting spectra are displayed in Fig. 5 (which we discuss in Section IV). (In Fig. 5 the elastic peak position minus the relevant core-level binding energy was taken as the zero reference value in each case.)

The data processing procedures we have described are based on the use of objective and, we feel, reasonable criteria. Evaluation of their adequacy, however, must rely on comparisons of our loss-corrected signals with integral signals from other probes of the CB DOS, and with theoretical calculations.

IV. RESULTS AND DISCUSSION

The $N(E)$ loss-deconvoluted CLIESS signals are plotted in Fig. 5 as functions relative to the Fermi energy (i.e., loss energy relative to threshold). These curves should be comparable with the results of other probes of the CB DOS for these materials and with theoretical DOS calculations where available. Soft x-ray absorption spectra form perhaps the most abundant source of reference spectra, especially for Al and Be.[21] In the last two decades CLIESS in transmission, using much higher primary beam energies than ours and requiring thin samples, has provided an alternative library of reference spectra.[5–7] Related data are found also in soft x-ray appearance potential spectroscopy (SXAPS)[22] and, more recently, Bremsstrahlung Isochromat Spectroscopy (BIS)[23] results.

We examine our Be(K) results first, because the extraction of the experimental CLIESS signals was straightforward, as we discussed in Sec. III. The extracted CLIESS line shape should be less distorted by errors in our analytic continuation of the plasmon-loss spectrum than may be the case for the Al(L$_{23}$) line shape. Table I depicts the locations of peaks in our Be(K)-CLIESS data, relative to a threshold value of 110.5 eV characteristic-loss energy. Also given are peak positions from SXAS measurements[3,24–26] and from two theoretical CB DOS calculations.[27,28] The results from two SXAPS studies of Be[29,30] are also included in this table. These latter data should be compared not with our $N(E)$ versus loss energy results but with the first (energy) derivative of $[N(E) \otimes N(E)]$, the self convolution of our $N(E)$ curve.[31] Our $d[N(E) \otimes N(E)]/dE$ peak positions are also given in the table. One sees that there are clear correlations between our results and those of others. In particular, our CLIESS peaks at 2.5, 7.5 and 13.9 eV are in good agreement in peak position with peaks in all SXAS and theoretical DOS curves.

The general line shapes of our spectrum and the comparison curves are also similar: we should note that the Be (K) results make it clear that loss-deconvolution removes much of the ''smearing'' associated with limits on system resolution. This similarity indicates that our CLIESS measurements for Be provide signals with line shapes that give the same information about the material as do SXAS measurements. Agreement with theoretical calculations indicates that this information is closely related to the CB DOS for the material.

The Al(L$_{23}$) curve in Fig. 5 can be compared to reports of an isochromat (and continuous) x-ray spectrum,[32] solid Al(L$_{23}$)[2,26] and Al(K)[33] and liquid Al(L$_{23}$)[34] SXAS data, Al(L$_{23}$) transmission CLIESS measurements[35] and calculations of the Al CB DOS.[36] Except for the Al(K) SXAS data, whose form differs from that of the Al(L$_{23}$) because of differing symmetry selection rules, all the data evince the rather featureless [compared to that of the Be (K)] behavior in Fig. 5: a continuous rise in intensity broken only by regions of near constant, or slowly increasing, intensity up to a loss energy of around 25.0 eV. Our derived CB DOS has an initial threshold step which is less steep than those reported for SXAS, which we attribute to inaccuracies in our plasmon-loss spectrum synthesis and not to a lack of resolution in our measurements, since our Be (K) threshold is quite sharp.

The SXAS[2,26] and transmission CLIESS[35] data and theoretical CB DOS results[36] show a strong minimum at around 28.0–30.0 eV loss energy, in contrast to the weak minimum in the vicinity of 30 eV loss energy in our data in Fig. 5. It is interesting to note that the shape in our data is actually closer to that of the Al(L$_{23}$) SXAS curve for liquid Al.[34] Apparently, the strong minimum is open to various, differing physical interpretations.[2,26,35,36] There is evidence from BIS data[37] for the minimum to be an artifact of the overlap between the primary spectrum and its plasmon replica.

In Fig. 5, we also present our results for Ni: we should

TABLE I. Comparison of our CLIESS results with spectra from other experimental probes of the conduction band DOS and with theoretical DOS calculations for elemental Be. The energy values are loss energies measured relative to the Be(K) threshold energy for the experimental data or energy above Fermi energy for the theoretical calculations. Our $N(E)$ results are compared on the left side of the table with SXAS results and with theoretical CB-DOS calculations. On the right side of the table our $d[N \otimes N]/dE$ results are compared with SXAPS data. ($[N \otimes N]$ denotes the convolution square of the function $N(E)$.) The ''Peak No.'' assignments are based on an arbitrary segmenting of the energy loss spectrum. The segments become larger with increasing loss energy as the experimental peaks become broader. The theoretical DOS calculations extended only ~ 18 eV and ~ 10 eV above the Fermi energy for Refs. 27 and 28, respectively. Peaks reported in the No. 7 peak window for SXAS and SXAPS were identified in the original references as due to extrinsic plasmon losses. Our loss-deconvolution processing is designed to remove such features.

	Soft x-ray absorption spectroscopy				Theoretical CB-DOS		Our CLIESS results		Soft x-ray appearance potential spectroscopy	
Peak No.	Ref. 3	Ref. 24	Ref. 25	Ref. 26	Ref. 27	Ref. 28	$N(E)$	$\dfrac{d[N \otimes N]}{dE}$	Ref. 29	Ref. 30
1	1.2 eV	1.2 eV	1.1 eV	1.2 eV	2.6 eV	2.2 eV	2.5 eV	2.5 eV	1.9 eV	1.9 eV
2	4.0 eV	⋯	3.9 eV	⋯	4.7 eV (weak)	4.5 eV (weak)	⋯	⋯	⋯	⋯
3	6.5 eV	⋯	6.4 eV	6.9 eV	7.0 eV	6.8 eV	7.1 eV	7.2 eV	7.0 eV	7.0 eV
4	10.2 eV	11.4 eV	10.2 eV	9.9 eV	9.0 eV (weak)	9.2 eV (weak)	10.7 eV (weak)	⋯	9.9 eV	11.4 eV
5	14.4 eV	⋯	13.3 eV	13.8 eV	11.1 eV	no data	13.9 eV	13.6 eV	13.0 eV	⋯
6	17.0 eV	⋯	⋯	⋯	15.0 eV	no data	⋯	⋯	⋯	16.3 eV
7	21.7 eV	⋯	21.2 eV	⋯	no data	no data	⋯	26.4 eV	21.1 eV	21.2 eV
8	27.0 eV	⋯	30.1 eV	32.7 eV	no data	no data	32.8 eV	39.9 eV	34.5 eV	37.2 eV
9	42.3 eV	48.5 eV	47.6 eV	48.0 eV	no data	no data	49.7 eV	51.2 eV	50.0 eV	46.5 eV

remark that the M_3 and M_2 peaks in our data are not resolved and that the start of the Ni(M_1)-CLIESS spectrum is superimposed on that of the Ni(M_{23}) curve after an extra energy loss of ~ 45 eV. Transmission CLIESS[38] and SXAS[39] measurements for the L_{23} absorption in nickel have been published. BIS has also been used[40] to probe the CB DOS of Ni more directly. The spectra from these measurements share features in common: an asymmetric peak at threshold followed by a more or less featureless tail at higher loss energies. This is, in general, what is seen in our Ni(M_{23})-CLIESS spectrum[19] in Fig. 5 and what is expected from the theoretical DOS[41] with the peak corresponding to the unfilled 3d-DOS levels and the tail resulting from a less dense but broad distribution of 4s CB levels.

Consideration of an early Ni(K) SXAS spectrum[42] suggests that our Ni curve would be more correct if it showed a step at threshold rather than a peak. This is what one might expect upon first examining our raw, derivative Ni data in Fig. 1. We should emphasize that this feature of the shape of our final $N(E)$ depends on the scaling used for the loss tail of the response function[19] in Fig. 3.

Finally, to help with the reader's assessment of our data processing procedures, Fig. 6 shows the 1st derivatives of the loss-deconvoluted curves in Fig. 5. A 21-point Savitzky–Golay, 1st derivative convolution array[16] was used to generate these curves, which, include some smoothing. One sees in a comparison between corresponding curves in Figs. 1 and 6 that, except in the circled region for Al and Be, the data

processing (1/E correction and loss deconvolution) produces only subtle changes in the characteristic features of the measured data. For the Al and Be data, the largest errors result-
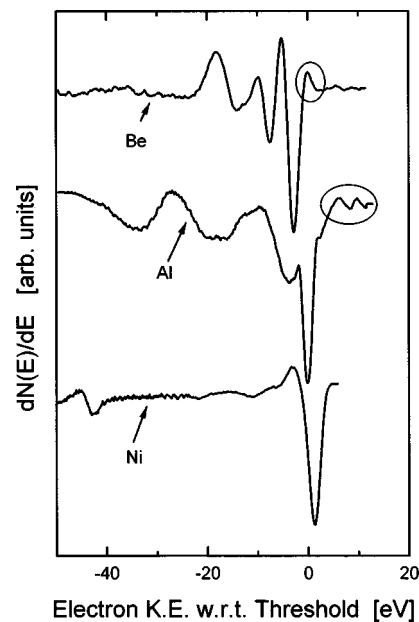

FIG. 6. First derivatives of the loss-deconvoluted spectra in Fig. 5. These curves should be compared with the corresponding curves in Figs. 1 and 4. The loss-deconvolutionenhanced errors from our plasmon simulations that occur near threshold for Be and Al have been circled.

ing from our procedures for separating the CLIESS signal from the overlapping plasmon spectra occur near threshold. These errors became enhanced in the loss deconvolution processing.

V. SUMMARY AND CONCLUSIONS

Absorption spectra of either x-ray photons or electrons give information about the outer, unoccupied electronic levels of solids. When the transitions involve a core level, this information becomes element specific. Much of the literature has involved transmission of probing beams through thin films. Investigation of the CB DOS information from the surfaces of solids has been less common. For SXAS, surface investigations rely on secondary detection schemes[43] that utilize the limited mean free paths of low energy electrons in solids. With high energy electron beams, surface sensitivity can, in principle, be obtained by performing CLIESS experiments in the reflection mode with glancing incidence. In practice, however, such experiments[44] have been found to be difficult.

Our CLIESS data presented in Fig. 5 were derived from data taken in the reflection mode, using low to medium energy incident beams. The loss spectra were recorded in the first-derivative mode, which mitigates the slowly varying background signal while enhancing the characteristic features of the spectra. For Al and Be, the strong plasmon-loss signals made the extraction of the core-level signals a problem. For Be, at least, a fairly good simulation of the plasmon-loss signals in the CLIESS energy region could be made. This evaluation is supported by the good agreement of features in our Be(K) loss-deconvoluted spectrum in Fig. 5 with the results of other experimental probes of the CB DOS of Be and with theoretical DOS calculations in Table I.

While Al and Be have strong plasmon-loss spectra expected of free-electron metals, their CLIESS signals are significantly different from being simply ''free-electronlike''. Their CLIESS signals are also clearly different from one another, making them useful for sample characterization. An indication of this sensitivity is presented in Fig. 2. The differences in their CB (CLIESS) spectra are greater than those found in their valence band (AES) spectra.[45,46] Even their plasmon-loss spectra are markedly different from one another, and from what one might expect for free-electron metals.

For the Ni(M_{23}) spectra (Figs. 1, 4 and 6), plasmon-loss features were not a problem. The major problem in this case was an uncertainty in the amount of loss-tail scaling that should be used in the loss-deconvolution processing.[19] The increased scaling used for the Fig. 5 results was chosen primarily to reduce the average upward slope in the loss-corrected spectrum after the threshold region. Compared with the scaling choice that one is faced with in dealing with AES data,[20] our choice here was somewhat arbitrary. The peak at threshold in our Ni(M_{23}) curve in Fig. 5 is closer in shape to the Ni(L_3/L_2) SXAS curve[39] and to the L_{23} CLIESS spectrum taken in transmission with 120 keV primary electrons[38] than it is to published Ni(K) SXAS data.[47]

This is entirely understandable for the SXAS results due to the fairly stringent selection rules in SXAS. The Ni(K) SXAS should not be expected to sample the narrow Ni d-electron distribution above the Fermi level. Our Ni(M_{23}) spectrum is also similar to the (noncore-level specific) Ni-BIS spectra.[40] One should note, however, that the strength of the initial peak in those BIS data varies greatly with the isochromat energy used.

Despite the fact that our loss-deconvoluted Al(L_{23}) CLIESS curve in Fig. 5 is the most suspect in terms of accuracy in shape, it is still similar to the Al(L_{23}) SXAS data[3,6] from solid Al up to about 25 eV loss energy. [It is less similar in shape to the Al(K)-SXAS spectrum.[48]] As noted above, however, our results are even closer in shape to the Al(L_{23})-SXAS spectrum for liquid Al.[34] The reason for this is not immediately clear.[49] Apart from the loss-deconvolution-enhanced errors just before threshold in our Al(L_{23}) curve, the major difference *vis a vis* the corresponding SXAS result for solid Al is in the absence of the pronounced minimum at $\sim$ 30 eV loss energy. The occurrence of this deep minimum gives the curve a strong peak maximum just below this loss energy. Whether this peak/ minimum structure should really be so strong is called into question by some BIS results,[37] suggesting that this structure is actually the result of an overlap of the primary spectrum with a replica spectrum shifted by the plasmon-loss energy. This type of spectral distortion is typical of what our loss-deconvolution technique is designed to remove from the ''as-measured'' data.

Our CLIESS results show that surface-sensitive CB DOS information may be obtained in systems designed for AES studies of solid surfaces. While the processing to which our data was subjected would not be necessary in order to follow changes in the surface CB DOS of a material, it is important to determine just what physical properties of the material govern the shapes of the spectra. These prove to be the same as those that govern corresponding spectral results from traditional bulk probes such as SXAS and transmission CLIESS. All these data are element specific, making them ideal probes of the local CB DOS about a given type of atom, and hence, of the local chemistry for that type atom in chemical compounds. This information comes not so much in terms of ''chemical shifts'' in threshold energies, but rather from the changes in shape of the spectral features.[14]

In this article, we have tried to formulate an objective procedure for extracting CB DOS information from the CLIESS. In the case of extraneous effects, such as plasmons in Al and Be, it was necessary to resort to empirical methods. We feel that these procedures have had some success in the cases of Al, Be and Ni. Extension of these objective, although somewhat empirical, prescriptions to other cases would not be especially difficult and would indicate their general utility.

ACKNOWLEDGMENTS

[1]D. Pines, Rev. Mod. Phys. **28**, 184 (1956).

[2]H. Raether, *Springer Tracts in Modern Physics* (Springer, Berlin, 1980), Vol 88, pp. 1–196.

[3]T. Sagawa, Y. Iguchi, M. Sasanuma, A. Ejiri, S. Fujiwara, M. Yokota, S. Yamaguchi, M. Nakamura, T. Sasaki, and T. Oshio, J. Phys. Soc. Jpn. **21**, 2602 (1966).

[4]For a short overview of SXAS, and of related techniques for CB DOS studies see: J. C. Fuggle and J. E. Inglesfield, *Topics in Applied Physics,* (Springer, Berlin, 1992), Vol. 69, pp. 1–24; and for a discussion of the theoretical approach(es) to understanding that part of the SXAS data, the near-edge structure, of relevance to our results, see P. J. Durham, in *X-Ray Adsorption: Principles, Applications, Techniques of EXAFS, SEX-AFS and XANES*, edited by D. C. Konigsberger and R. Prins (Wiley, New York, 1988), pp. 53–84.

[5]L. Marton, L. B. Leder, and H. Mendlovitz, Adv. Electron. Electron Phys. **7**, 183 (1955).

[6]S. E. Schnatterly Solid State Phys. **34**, 275 (1979).

[7]R. F. Egerton, *Electron Energy-Loss Spectroscopy in the Electron Microscope* (Plenum, New York, 1986).

[8]J. Fink, Adv. Electron. Electron Phys. **75**, 121 (1989); *Topics in Applied Physics* (Springer, Berlin, 1992), Vol. 69, pp. 203–241.

[9]W J. Pardee, W. D. Mahan, D. E. Eastman, R. A. Pollak, L. Ley, F. R. McFeely, S. P. Kowalczyk, and D. A. Shirley, Phys. Rev. B **11**, 3614 (1975).

[10]P. M. Th. M. van Attekum and J. M. Trooster, Phys. Rev. B **18**, 3872 (1978).

[11]P. Steiner, H. Höchst, and S. Hüfner, Z. Phys. B **30**, 129 (1978); A. Bernhard, Fr. Reinert, Th. Engel, P. Steiner, and S. Hüfner, Deutsche Physik. Gesellschaft Tagung, Münster, Germany, 1993 Abstract O-18.6; A. Bernhard, Diplomarbeit thesis, 1994.

[12]F. Yubero and S. Tougaard, Phys. Rev. B **46**, 2486 (1992); Surf. Interface Anal. **19**, 269 (1992).

[13]Because of a potassium impurity in our Al source material, the W substrate was held at T=600–675 K during the deposition of Al. This allowed Al films to be deposited while keeping K levels below AES detection limits. For the results presented here, the Ni films were deposited onto oxidized Al films. Deposition of clean Ni was continued until there was no AES evidence of the underlying aluminum or oxygen.

[14]H. H. Madden, R. Landers, G. G. Kleiman, and D. M. Zehner (in preparation).

[15]T. Aiyama and K. Yada, J. Phys. Soc. Jpn. **36**, 1554 (1974).

[16]H. H. Madden, Anal. Chem. **50**, 1388 (1978). Convolution arrays for smoothing were calculated using Eq. II in Table I of this reference. The 1st derivative arrays were calculated using Eq. V.

[17]P. H. van Cittert, Z. Phys. **69**, 308 (1931).

[18]H. C. Burger and P. H. van Cittert, Z. Phys. **79**, 722 (1932); **81**, 428 (1933).

[19]For a discussion of loss deconvolution see Ref. 21. The ''proper'' amount of losstail scaling for processing AES data is guided by the criterion that Auger signals should be finite in energy width, so that they should approach zero intensity smoothly around 10–15 eV below the high energy thresholds. Such behavior reduces the average upward slope in the loss-corrected spectrum after the threshold region. For Ni, this required that we increase the strength of the loss tail of the experimentally measured

system response function (see Fig. 3). The system response functions for Be and Al loss deconvolution in Fig. 3 were found to satisfy this criterion as measured, so that no scaling of the loss tail was done in either of these two cases. We should note that the shape of the final $N(E)$ spectrum is sensitive to the scaling used for the loss tail of the response function (e.g., for Ni, utilizing no scaling produces a step at threshold, in contrast to the peak in Fig. 5).

[20]H. H. Madden, Surf. Sci. **126**, 80 (1983); H. H. Madden and J. E. Houston, J. Appl. Phys. **47**, 3071 (1976).

[21]For a bibliography of references covering SXAS investigations to 1987/88, see: A. Meisel, G. Leonhardt, and R. Szargan, *X-Ray Spectra and Chemical Binding,* Springer Series in Chemical Physics (Springer, Berlin, 1989), pp. 345–451.

[22]O. W. Richardson and C. B. Bazzoni, Philos. Mag. **42**, 1015 (1921); R. L. Park, J. E. Houston, and D. G. Schreiner, Rev. Sci. Instrum. **41**, 1810 (1970).

[23]J.C. Fuggle, *Topics in Applied Physics* (Springer, Berlin, 1992), Vol. 69, pp. 307–337.

[24]A. P. Lukirskii and I. A. Brytov, Sov. Phys. Solid State **6**, 33 (1964).

[25]N. Swanson and K. Codling, J. Opt. Soc. Am. **58**, 1192 (1968).

[26]R. Haensel, G. Keitel, B. Sonntag, C. Kunz, and P. Schreiber, Phys. Status Solidi A **2**, 85 (1970).

[27]T. L. Loucks and P. H. Cutler, Phys. Rev. **133**, A819 (1964); an extended CB DOS curve from these authors is presented in Ref. 2 above.

[28]P. O. Nilsson, G. Arbman, and T. Gustafsson, J. Phys. F **4**, 1937 (1974).

[29]P. O. Nilsson and J. Kanski, Surf. Sci. **37**, 700 (1973).

[30]A. M. Bradshaw and W. Wyrobisch, J. Electron Spectrosc. Relat. Phenom. **7**, 45 (1975).

[31]See review articles: R. L. Park and J. E. Houston, J. Vac. Sci. Technol. **11**, 1 (1974); A. M. Bradshaw, in *Surface and Defect Properties of Solids*, edited by M. W. Roberts and J. M. Thomas (Chemical Society, Burlinghouse, London, 1974), Vol. 3, pp. 153-183.

[32]S. Nishiyama and H. Fujimoto, J. Phys. Soc. Jpn. **36**, 1614 (1974); for more recent Al-BIS spectrum see Fig. 10.9 in Ref. 24 above.

[33]I. Nagakura, Sci. Rep. Res. Inst. Tohoku Univ. A **48**, 37 (1964) (as reported in Fig. 3 of Ref. 2 above).

[34]H. Petersen and C. Kunz, Phys. Rev. Lett. **35**, 863 (1975).

[35]J. J. Ritsko, S. E. Schnatterly, and P. C. Gibbons, Phys. Rev. Lett. **32**, 671 (1974).

[36]J. W. D. Connolly, Int. J. Quantum Chem. **IIIs**, 807 (1970).

[37]In Ref. 24, see Figs. 10.9 and 10.10.

[38]N. J. Zaluzec, Ultramicroscopy **9**, 319 (1982).

[39]C. T. Chen, F. Sette, Y. Ma, and S. Modesti, Phys. Rev. B **42**, 7262 (1990).

[40]W. Speier, J. Phys. C: Solid State Phys. **21**, L1183 (1988).

[41]V. L. Moruzzi, J. F. Janak, and A. R. Williams, *Calculated Electronic Properties of Metals* (Pergamon, New York, 1978).

[42]T. Shiraiwa, T. Isimura, and M. Sawada, J. Phys. Soc. Jpn. **13**, 847 (1958).

[43]A. Bianconi, in *X-Ray Absorption: Principles, Applications, Techniques of EXAFS, SEXAFS and XANES,* edited by D. C. Konigsberger and R. Prins (Wiley, New York, 1988) pp. 537–662.

[44]O. L. Krivanek, Y. Tanishiro, K. Takayanagi, and K. Yagi, Ultramicroscopy **11**, 215 (1983).

[45]J. E. Houston, J. Vac. Sci. Technol. **12**, 255 (1975); and unpublished results.

[46]D. R. Jennison, H. H. Madden, and D. M. Zehner, Phys. Rev. B **21**, 430 (1980).

[47]D. M. Pease and T. K. Gregory, Solid State Commun. **18**, 1133 (1976).

[48]C. Sénémaud, Phys. Rev. B **18**, 3930 (1978); see also Fig. 6.24 (p. 248) in Ref. 22 above.

[49]The liquid Al results were obtained using electron-yield detection methods. Thus, one might at first suspect that increased surface sensitivity rather than the lack of crystalline order is the basis for this similarity. That this cannot be the answer is seen in the fact that this same SXAS experimental setup was used (Ref. 34) to measure spectra for solid samples and these spectra agree with more traditional Al(L$_{23}$)-SXAS results for solid Al.